Pergamon

Canadian Metallurgical Quarterly, Vol. 37, No. 3-4, pp. 197 212, 1998

0008-4433/98 $19.00+0.00

PII: S0008-4433(98)00025-1

MODELING OF TRANSIENT FLOW PHENOMENA IN CONTINUOUS CASTING OF STEEL

X. HUANG† and B. G. THOMAS*‡

† Concurrent Technologies Corporation, 1450 Scalp Ave, Johnstown, Pa 15904, U.S.A.
‡ Department of Mechanical and Industrial Engineering, University of Illinois at Urbana-Champaign, 1206 West Green Street, Urbana, IL 61801, U.S.A.

(*Received* 19 *August* 1996; *in revised form* 8 *June* 1998)

Abstract—This paper describes initial efforts to develop and apply 3D finite-difference models to simulate transient flow in the mold. These transient flow phenomena include flow pattern oscillations caused by sudden changes in nozzle inlet conditions and rapid fluctuations in the molten steel/flux interface level at the top surface of the mold. The flow model incorporates interactions with other transport phenomena, including turbulence, superheat removal and argon gas bubble injection. Predictions are shown for the oscillatory evolution of the flow pattern from biased steady flow to symmetrical steady flow after a sudden change in inlet conditions. In addition, the predicted turbulent kinetic energy levels at steady state are shown to correlate with measured surface level fluctuations. The effect of processing conditions are consistent with experimental findings. Without argon, the greatest level fluctuations are found near the narrow face, while increased argon moves the maximum towards the center. Fluctuations decrease with deeper submergence and lower casting speed. These transient phenomena are important because they may lead to defects in the final steel product from entrainment of slag, disruption of solidification at the meniscus and non-uniform heat transfer. © 1998 Canadian Institute of Mining and Metallurgy. Published by Elsevier Science Ltd. All rights reserved.

Résumé—Ce document décrit les efforts initiaux de développement et d'application de modèles aux différences finies en 3D à la simulation de l'écoulement transitoire dan le moule. Ces phénomènes d'écoulement transitoire incluent les oscillations du patron d'écoulement causées par des changements de conditions de la tuyère d'entrée ainsi que les fluctuations rapides du niveau de l'interface acier fondu/écoulement à la face supérieure du moule. Le modèle d'écoulement incorpore des interactions avec d'autres phénomènes de transport, incluant la turbulence, l'enlèvement de la surchauffe et l'injection de bulle de gas d'argon. On prédit l'évolution oscillatoire du patron d'écoulement, allant d'un écoulement permanent biaisé à un écoulement permanent symétrique, après un changement soudain des conditions d'entrée. En plus, on montre que les niveaux prédits d'énergie cinétique turbulente en régime permanent sont corrélés avec les valeurs mesurées de fluctuations du niveau de la surface. L'effet des conditions du traitement est consistant avec les données expérimentales. San argon, le niveau le plus élevé de fluctuations se situe près de la face étroite alors que l'augmentation d'argon déplace le maximum vers le centre. Les fluctuations diminuent avec une immersion plus profonde et une vitesse de moulage plus lente. Ces phénomènes transitoires sont importants parce qu'ils peuvent conduire à des défauts dan le produit final en acier par entraînement de scories, par dérangement de la solidification au ménisque et par transfert de chaleur non uniforme. © 1998 Canadian Institute of Mining and Metallurgy. Published by Elsevier Science Ltd. All rights reserved.

INTRODUCTION

The process of continuous casting is most efficient and produces the highest quality product when operated at steady state. Unfortunately, it is subject to several different types of transient phenomena. These include transitional transients, periodic oscillations and random fluctuations due to turbulence. This paper applies mathematical models to explore some of the transient phenomena which affect the continuous casting of steel slabs.

Casting conditions are often upset intentionally, for example, the casting speed is slowed down and then ramped up to desired operation value when the ladle, or tundish, or both are replaced during a grade change [1]. The casting speed is also lowered to change the submerged entry nozzle (SEN), or when the mold width is changed during operation [2, 3]. This kind of transient process can be classified as transitional transient phenomena because the system normally returns to steady state after several minutes. Other transient phenomena are of a periodic nature. These include the vertical movement of the mold during each oscillation cycle [4] and the periodic bulging of the strand as it moves between rolls [5]. Finally, random changes associated with turbulence are almost intrinsic in the mold region of steel casters due to the nature of fluid flow in this regime. Turbulence contributes to fluctuations of the surface level of the liquid pool [6]. In the extreme, severe sloshing may occur, which has been observed in a water model of a thin slab caster [7]. The magnitude of these turbulence effects likely depends on casting

* Author to whom correspondence should be addressed.

conditions, which include casting speed, argon injection rate, nozzle submergence depth, mold geometry and nozzle geometry.

Understanding transient phenomena is important because they can significantly affect steel quality. Surface level fluctuations in the mold may lead to defects by disrupting mold flux infiltration and solidification at the meniscus. This can lead to the entrapment of slag [8], surface depressions [9–11] and cracks [11, 12] due to the associated non-uniform heat transfer between the strand and the mold [6, 13]. More severe damage may be caused by violent changes in the melt pool during system sloshing. In extreme cases, transient phenomena can lead to a costly break-out, for example, during an inappropriate adjustment of mold width [2].

A few previous efforts to model transient behavior in continuous casting processes can be found in the literature. Finite-difference mixing models have been developed to predict the transient change of steel concentration in the tundish and strand during steel grade changes [1, 14–17]. Melt velocities and temperatures were assumed to be steady state so that only steel compositions varied with time. The predicted slab concentration at tundish outlet [1, 14–17] and slab compositions [1, 14, 15] agree well with tundish water model measurements and plant trials. Research efforts have also been devoted to developing fully-transient fluid-flow and heat-transfer models and applying them to transient phenomena in continuous casting ladles [18] and tundishes [19]. The transient Navier–Stokes' equations, along with the standard K–ε turbulence model, were solved to obtain fluid flow velocities and temperatures. A recent finite element stress analysis [11] was performed to predict the effect of a sudden fluctuation in liquid level on distortion of the solidifying shell. The results illustrated how thermal distortion during a level drop can contribute to the formation of transverse surface depressions and short longitudinal surface cracks.

Although experimental measurement of transient phenomena in an operating continuous casting machine are very difficult, researchers have dedicated great effort to these phenomena to improve steel quality by reducing or eliminating related defects. Recent work [13] includes the successful application of a magnetic field to reduce power slag inclusions in high speed continuous slab casting. Since measurements of the liquid level fluctuations in a water model have shown a linear correlation with the melt velocity, a traveling magnetic field was imposed to stabilize and control meniscus surface flow. Surface level fluctuations were kept below 6–9 mm, slag entrainment was avoided and corresponding surface defects on the rolled product were reduced. Similar work was reported earlier by Teshima *et al.* [6]. Liquid level fluctuation in the steel continuous casting mold and in the corresponding water model were measured with an eddy current distance meter and a Laser distance meter respectively. Level fluctuations were then empirically correlated to casting conditions, such as casting speed, mold geometry, SEN nominal angle and submergence depth, steel properties and argon injection rate. The results were successfully applied in a Fukuyama caster and produced a superior surface quality of slabs cast at high speed up to 50 mm/s (3 m/min).

The first objective of this paper is to develop a transient 3D finite difference model to simulate unsteady flow phenomena caused by a sudden change in casting conditions. Secondly, the turbulent kinetic energy predicted by both transient and steady state models are analyzed to explore the correlation between turbulence and liquid level fluctuation. Finally, the interaction of transient behavior with casting parameters, such as argon injection, casting speed, and SEN submergence depth, are examined.

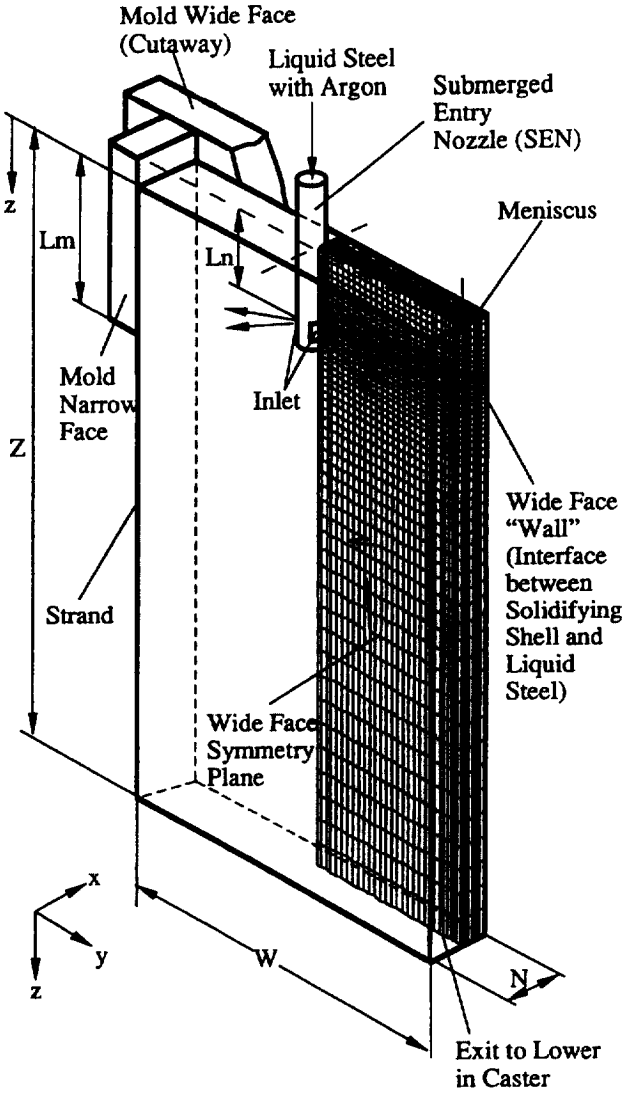

Fig. 1. Schematic diagram of 1/4 mold and stand simulation domain with typical mesh.

TRANSIENT TWO-PHASE FLOW AND HEAT TRANSFER MODEL

Figure 1 illustrates the portion of the slab casting mold and strand considered in the present work. A rectangular computational domain is placed up to solid-liquid interface (or mush region) to include a 3 m long liquid pool within the solid shell. Often only one quarter of the mold needs to be modeled because of twofold symmetry. In this work, one half of the mold is modeled in some cases in order to investigate the asymmetric nature of flow about the narrow face centerplane. Asymmetric

flow about the wide face centerplane, due to nozzle misalignment directing flow toward the mold corners, has been modeled elsewhere [20].

A transient two-phase flow and heat transfer model has been developed for this chosen domain based on a finite-volume numerical algorithm. Argon gas bubbles and their effects on the fluid flow and head transfer were taken into account in the model. This multiphase model accounts for the phenomena of bubble buoyancy with drag, bubble dispersion in the flow field, and the effect of the rising bubbles on the flow field. A single set of equations of mass continuity, momentum, energy transport and a modified two-equation K–ε turbulence model, were solved for the mixture of molten steel and carried bubbles. Essentially, the bubble motion is described by superimposing the bubble terminal velocity, defined as the bubble final rising velocity in a static ambient fluid, onto the liquid velocity field. Consequently, no momentum equation is solved in this work for the bubble phase. Instead, the bubble velocity at each location was calculated by adding its terminal velocity, v_{gt}, to the corresponding liquid velocity.

The size range of the bubbles used in the continuous steel casting processes is assumed to be less than 5 mm. Previous published research [21] showed that such small bubbles heat up and expand from room temperature to the liquid steel temperature in the SEN before they enter the mold. The hydrostatic pressure change is relatively small in the upper portion of the liquid pool. Thus, it was assumed in this work that the temperature and corresponding volume of each bubble is constant. Furthermore, thermal buoyancy forces in the molten steel were ignored, based on the justification provided in previous work [21].

The model is based on work found in several other references [21–31]. Details regarding the model equations are provided in Appendix I.

Blockage technique for nozzle volume

The typical core diameter of the SEN is about 0.125 m, which occupies more than half of the mold cavity thickness, which is typically 0.200 m. Most previous models have ignored the effect of the volume taken by the SEN [1, 21, 32]. In this work, its effect was taken into account for half-mold simulations by modeling the nozzle as a solid block in the mold cavity. Velocities inside the nozzle were fixed to zero. Flow velocities and turbulence parameters were imposed on the two inlet planes corresponding to the nozzle ports. This blockage technique creates no extra numerical difficulty, but is conceptually more accurate.

Boundary conditions

Inlet conditions. One half of the mold is included in the computational domain for the transient simulation. For this case, there are two inlet planes corresponding to the two outlet ports of the bifurcated SEN. For the other cases, only a quarter of the mold cavity is modeled, so only one inlet plane is imposed at the narrow face symmetry centerplane. At the inlet plane(s), all of the velocity components, turbulent kinetic energy and dissipation rates, are specified based on the output of a separate model of the nozzle [33]. Bubble parameters at the inlet plane(s) were fixed at a uniform value and temperature was imposed at the steady-state pouring temperature.

Outlet plane. At the outlet plane of the computational domain, 3 m below the meniscus, the normal gradients of velocities, turbulent quantities, temperature and bubble volume fraction (if applicable), are all set to zero. This assumes that the variation of these variables along the casting direction is negligible at this depth.

Symmetry planes. Normal velocity components and normal gradients of the other dependent variables, including tangential velocities, turbulence quantities, temperature and bubble fraction are set to zero for the wide face symmetry plane for all cases. The same conditions are imposed on the narrow symmetry plane when a quarter of the mold cavity is simulated.

"Wall" boundaries. To avoid the computational difficulties associated with modeling latent heat evolution at the solidification front, fluid flow is modeled up to, but not including, the mushy zone. The boundaries of the mesh along the narrow and wide face walls then correspond to the dendrite tips forming the outer limit of the mushy zone. Consequently, a fixed temperature, nominally equal to the liquidus, T_{liq}, is imposed along the narrow and wide face mold walls, which should behave like a rough solid wall. To account for the steep gradients that exist near the walls, empirical "wall law" functions [22, 23, 34] are employed to define the tangential velocities, turbulent quantities, and temperature at the near-wall grid nodes. Bubble volume fraction gradient is set to zero.

Top surface. The top surface is treated like a symmetry plane, except for temperature and bubble fraction. Heat lost via conduction and radiation through the molten flux and powder layers was modeled using an effective heat transfer coefficient ($h_a = 40$ W/m^2 °K) and ambient temperature ($T_\infty = 300$ °K), taken from previous work [35]. A parametric study showed that changing this heat transfer coefficient has only a slight effect on the overall results, as the top surface behaves close to an insulated boundary. Bubbles, if applicable, were assumed to escape from the top surface at their terminal velocities. Thus, the resistance of the viscous liquid flux layer acting to impede both the tangential steel velocity and the normal bubble rising motion was neglected. Finally, variations in the free surface position were ignored, as the effect on flow is believed to be negligible for most cases.

Numerical procedures A semi-implicit finite-volume formulation, SIMPLE algorithm, was chosen to solve this non-linear coupled problem. The differential equations and boundary conditions were discretized into a staggered mesh, which prevents false wiggled solutions. To aid convergence, an upwinding scheme was employed for the advection terms in regions with a high cell Reynolds number [22]. In addition, the source terms were linearized to increase diagonal dominance of the coefficient matrix [22]. The equations were solved with an Alternating-Direction-semi-Implicit iteration scheme consisting of three successive Tri-Diagonal-Matrix-Algorithm solutions (one for each coordinate direction) [22].

For the transient simulation, a fully implicit backward Eulerian scheme was adopted for time discretization. The direct successive iteration of the SIMPLE algorithm was applied within each time step using an under-relaxation factor of 0.2 or 0.3 until the maximum relative residual error and maximum

Table 1. Simulation conditions for the transition from uneven flow to even flow (without argon gas)

Parameters	Values
h_a, heat transfer coefficient at top surface	40 W/m^2 K
k_{01}, steel molecular conductivity	26 W/m K
K_0, turbulent kinetic energy at mold inlet	0.0502 m^2/s^2
SD, SEN submergence depth	0.265 m
SEN diameter	0.127 m (5 in)
W, mold width	1.32 m (52 in)
N, mold thickness	0.203 m (8 in)
T_∞, ambient temperture	27°C
T_0, pouring temperture	1550°C
v_c, casting speed	16.7 m/s (1.0 m/min)
α_0, nominal angle of nozzle port	25°
ε_0, turbulence dissipation rate at mold inlet	0.457 m^2/s^3
μ_{01}, steel laminar viscosity	0.0055 kg/ s m
ρ_l, liquid steel density	7020 kg/m^3

relative error between successive solutions fell below 0.1%. Variable time steps were taken to ensure a relative time truncation error of 0.1%. A simulation of 200 s of casting requires about 30 time steps and 40 h of CPU time on an IBM RS6000 workstation (100 h on an SGI IRIS/35) for a $60 \times 42 \times 12$ mesh. About one quarter of this CPU time, i.e. 10 h, is needed for a steady state simulation using the same mesh.

PREDICTION OF A TRANSITION FROM UNEVEN TO EVEN FLOW

The 3D, 2-phase flow model was first used to explore how uneven and sudden changes in inlet flow conditions affect the evolution of transport phenomena in the liquid steel pool. The initial condition was a steady-state flow pattern with a "biased flow" of 67% through the right port and 33% through the left port (see Table 1). It is commonly believed that such flow conditions are detrimental to steel quality, leading to increased nonuniformity in heat transfer and increased likelihood of internal entrapment of detrimental inclusions into the solidifying shell. It is not known whether these problems are due to the biased nature of this particular steady flow pattern itself, or to the unstable transient flow conditions which are associated with it.

At time = 0, flow through the nozzle ports was suddenly made uniform, with 50% of the flow exiting through each port. Transient calculation were then performed to simulate the transition of the flow pattern back to a new steady state condition. The type of event simulated here, which suddenly reduces asymmetry through the nozzle, could be caused by a sudden change in slide gate position, the sudden release of a nozzle clog, a realignment of the nozzle, realignment of the stopper rod in the tundish, or some other event. During the transient simulation, the normal velocity components, turbulence quantities and temperature were all fixed to the same values through each port. However, the tangential boundary condition was changed to zero shear stress. This released the tangential velocity components to allow the jet angle to change freely as the flow transition developed.

Steady biased flow results

Figure 2 a) illustrates the first result of interest: the initial asymmetric flow on opposite sides of the mold width, which has been observed previously in water models. Biased flow through the inlet greatly affects velocities in the upper recirculation zones in the mold. In this case, it causes stronger flow in the upper right. The top surface velocity on the right side reaches 0.07 m/s, which is more than triple the maximum on the left side, 0.02 m/s. This will aggravate the entrainment of molten flux globules from the right surface.

In addition, the biased flow greatly changes the relative size of the large vortices in the lower strand, or "lower recirculation zones". The stronger right jet entrains much more liquid, which greatly enlarges the lower right recirculation zone. This is because momentum entrainment by the incoming jet is proportional to the square of the jet velocity, resulting in four times more momentum directed to the right. Liquid flows downward to the lower strand through only about a quarter of the width at the mold exit depth. This will lead directly to the deep penetration of inclusions and bubbles causing subsurface defects that predominate on the right hand side of the strand.

This biased flow pattern produces a corresponding bias in the turbulent kinetic energy and temperature fields, as illustrated in Figs 3 a) and 4 a). Specifically, K and T are higher on the right side, as expected. A corresponding increase in surface level fluctuations is predicted on the right side, with a corresponding aggravation of surface defects on that side.

The upper recirculation zones have similar shape and size. This reflects the important influence that the nozzle has in blocking flow between the two halves of the upper mold. Even though the nozzle takes only 62% of the thickness cross section, (0.127 out of 0.203 m) it allows only a very weak cross flow from right to left along the top surface.

Transient results

Figures 2–4 show the time evolution of steel velocity, turbulent kinetic energy, and temperature viewed at the wide face centerplane. As time elapses, the lower left vortex at the left hand side grows and becomes one of the twin vortices when the flow approaches the symmetrical steady state. An interesting observation is that the small steady vortex that eventually forms on the lower right does not evolve by shrinking of the initially large lower right recirculation zone. Instead, this initially large vortex is shed away from the nozzle after about 17 s (Fig. 2 c). It gradually loses its swirling momentum as it moves downwards deep into the lower strand, (Fig. 2 d), where it eventually dissipates. At the same time, another vortex emerges on the right hand side at 17 s (Fig. 2 c). It gradually grows to match the size of its left partner to form the steady twin-vortex flow pattern (Fig. 2 f).

As the large vortex sheds in the lower region, a left-right oscillation in the flow pattern is created. The lower left vortex in Fig. 2 a) enlarges for the first 27 s, extending over the right side of the mold from Fig. 2 a) to d). It later shrinks back, to equal its right partner. The influence of this oscillation extends to the flow beyond 3 m below the meniscus. Liquid leaves the domain mainly from the left for the first 7 s, Fig. 2 a) and b), switches its preference to the right half after 17 s, Fig. 2 c), and finally becomes equal after about 92 s, Fig. 2 f). These damped

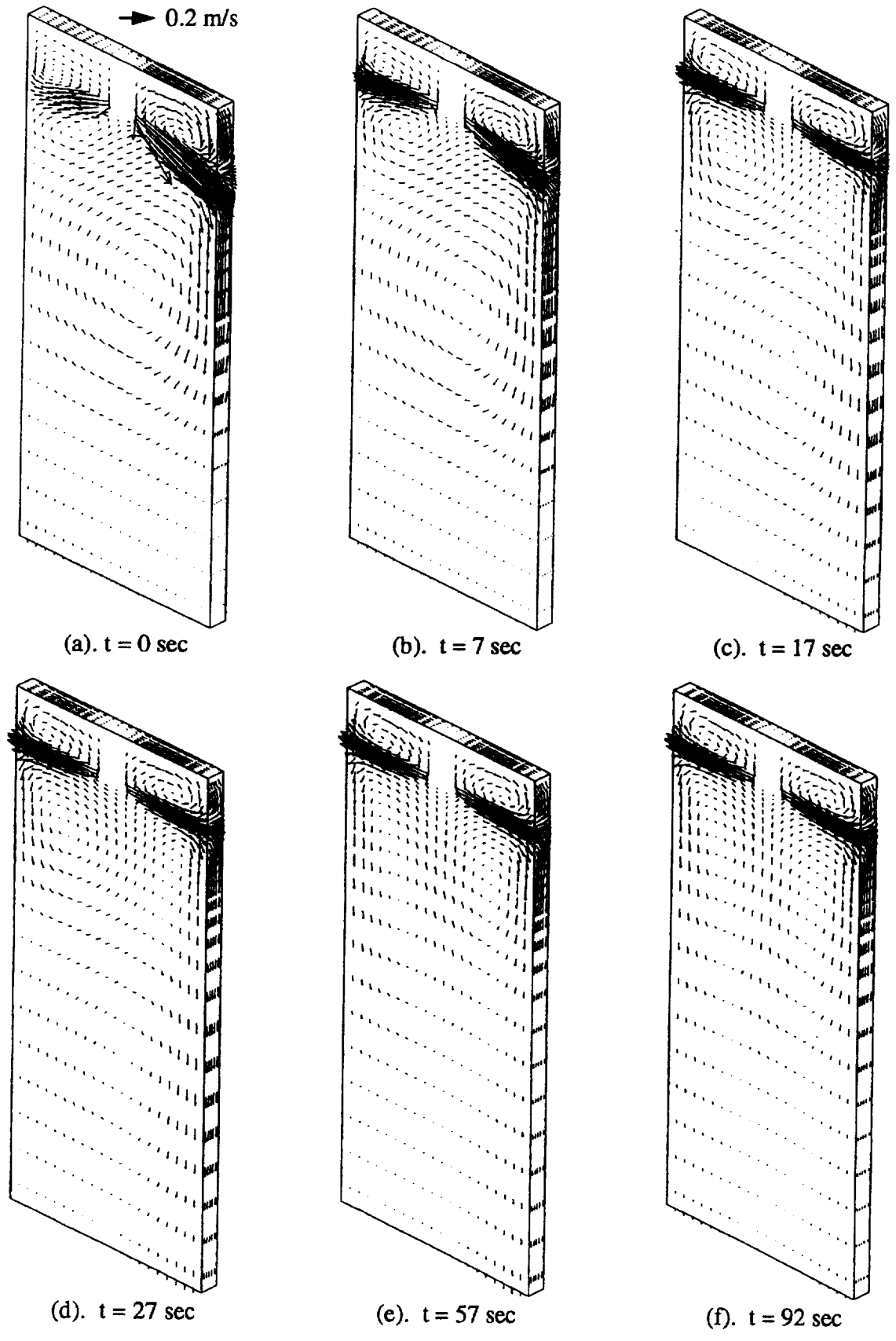

Fig. 2. Predicted evolution of velocities for simulation conditions in Table 1.

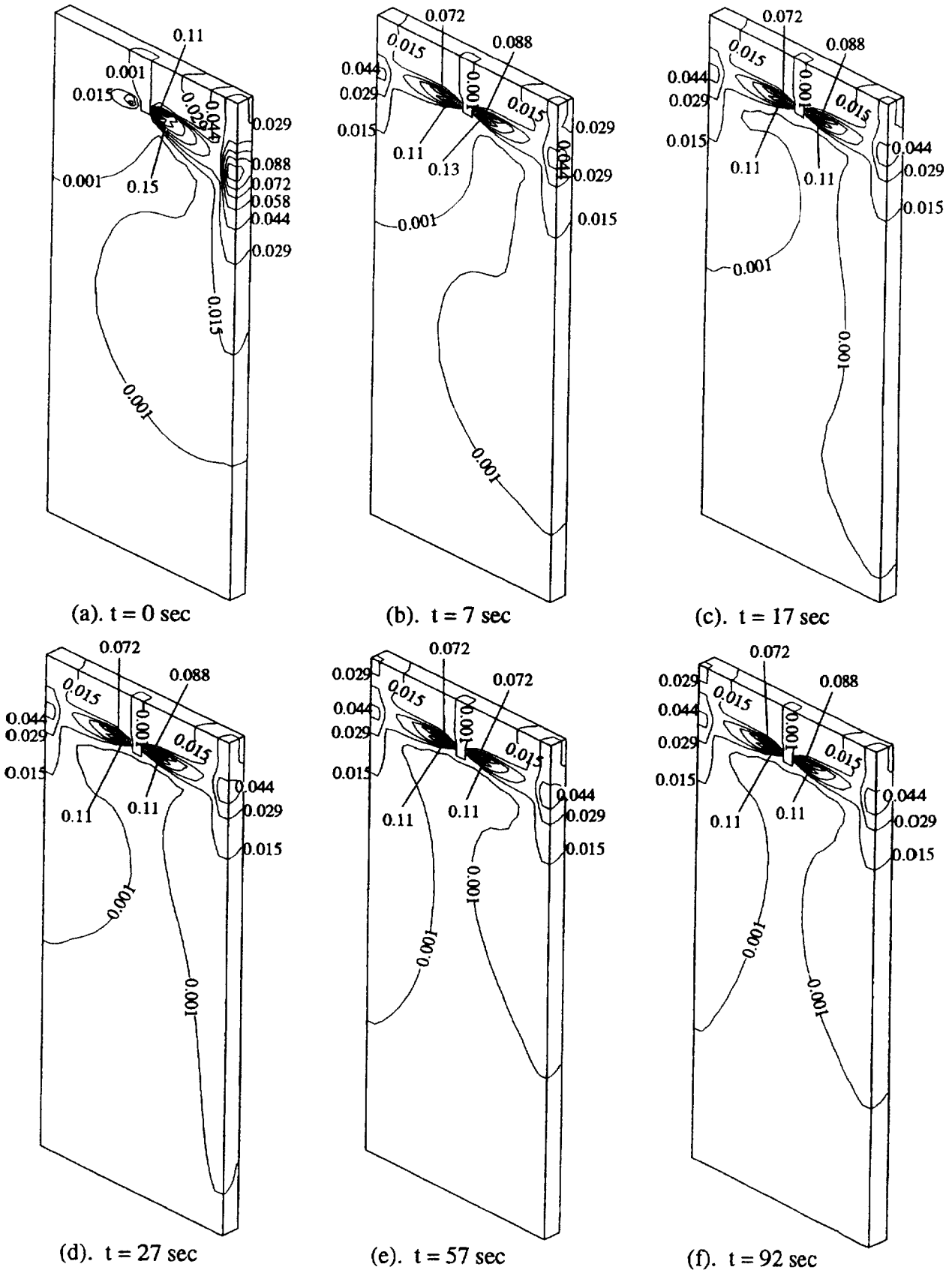

Fig. 3. Predicted evolution of turbulent kinetic energy for conditions in Table 1 (label unit m^2/s^2).

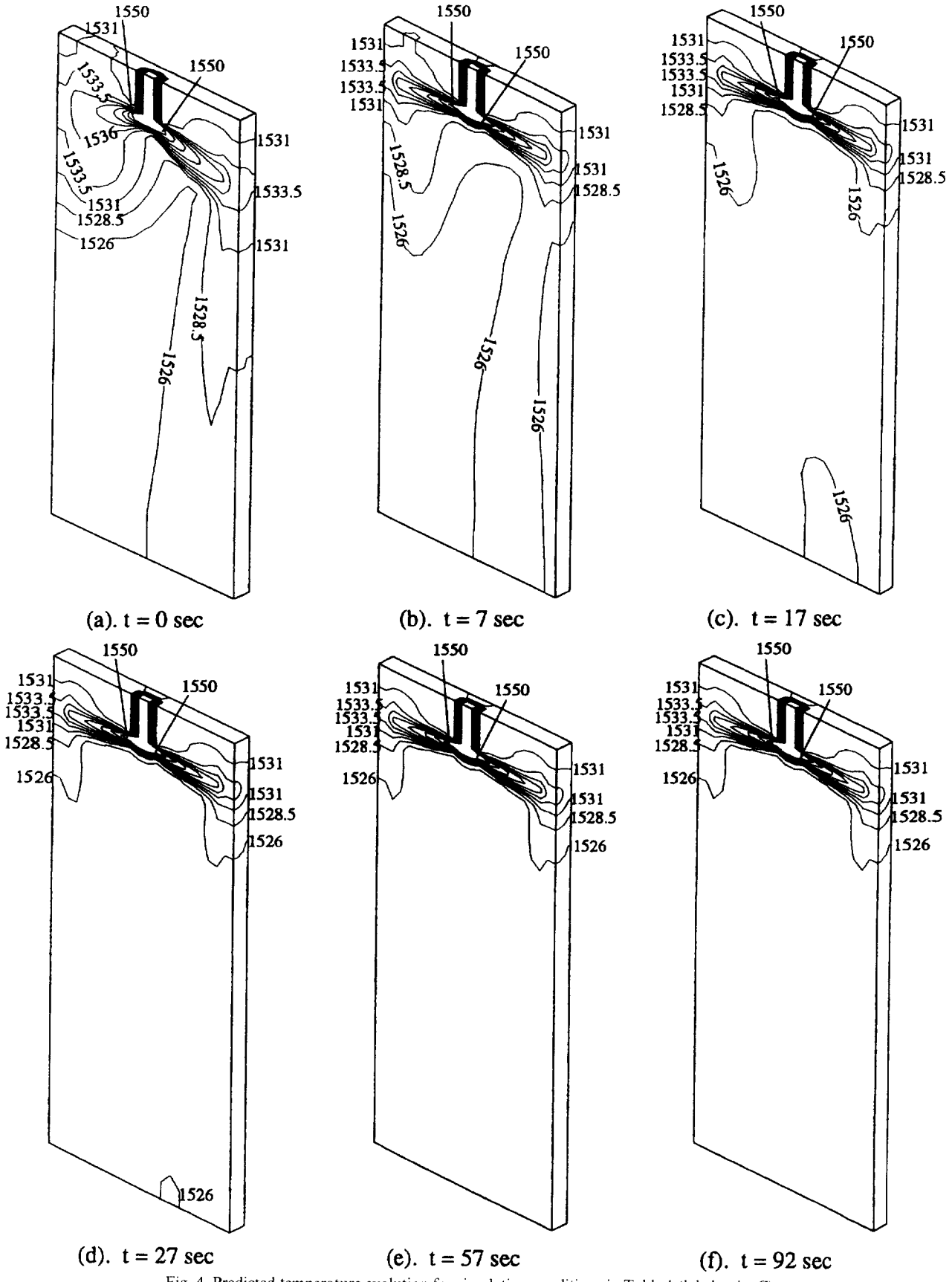

Fig. 4. Predicted temperature evolution for simulation conditions in Table I (label unit C).

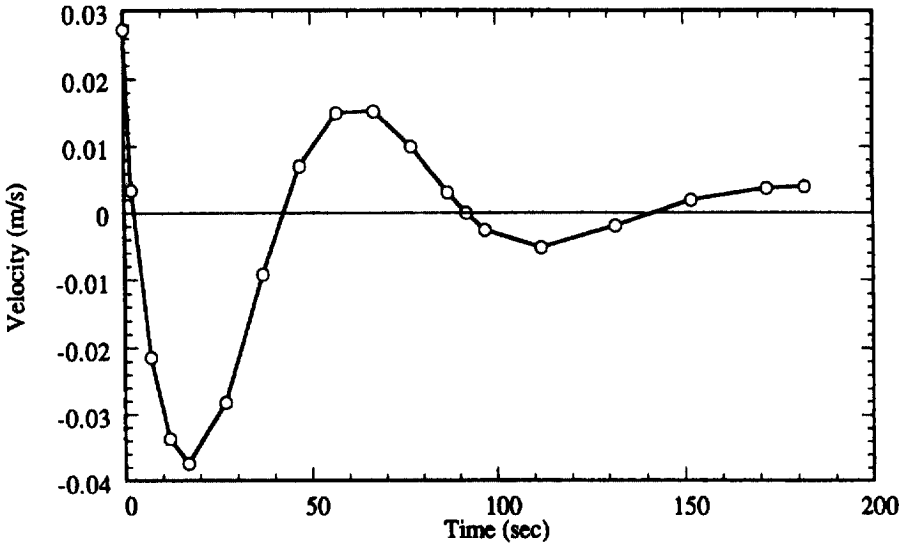

Fig. 5. Variation of melt y-velocity vs time at 2 mm below nozzle bottom on mold centerline.

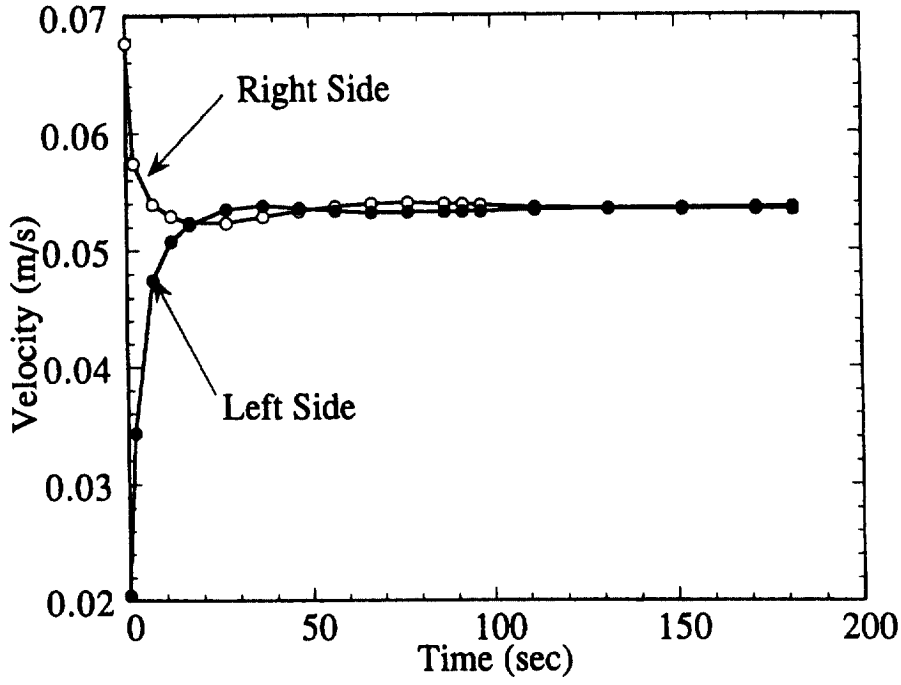

Fig. 6. Variation of melt y-velocity vs time at the meniscus.

oscillations are also illustrated in Figs 5 and 6. It is suspected that these oscillations are stronger in the steel caster than they are in the model predictions, which are dampened by numerical diffusion. Asymmetric flow across the centerline (Fig. 5) is seen to approach its steady value of 0 after only 200 s. The period of each oscillation cycle is about 90 s (1.5 min), which is also expected in the steel caster. This vortex shedding phenomenon may explain the time-variation in sizes of the lower recirculation zones observed in water models [36, 37].

The final steady flow field (Fig. 2 f) is interesting: the jet angle leaving the ports becomes horizontal. This result is not usually obtained in practice, however, as the angle of the jet entering the mold is determined primarily by the angle of the nozzle ports. It is interesting to consider that a horizontal inlet angle might lessen the oscillation and create more stable flow in the mold.

Surface pressure at the meniscus along the wide face centerplane is shown in Fig. 7. This distribution on the artificially-imposed top surface plane may provide an index for estimating the shape of the top free surface of the molten pool. In reality,

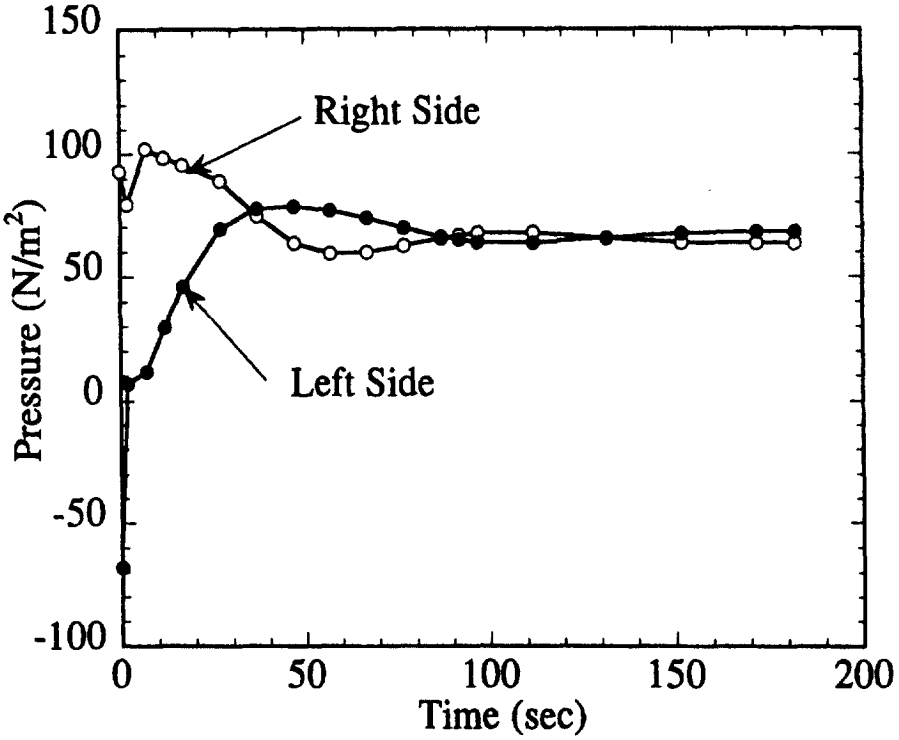

Fig. 7. Variation of pressure vs time at the meniscus.

this pressure is reduced by raising the surface level, H, until it balances the small steel surface tension. Experimentally measured melt-flux interfaces [38–40], i.e. steel top surfaces, show the same shape as the pressure predicted by the numerical model. This implies a strong correlation between the two. The quantitative relationship was difficult to establish, however, due to the difference between dynamic pressure calculated by the model, and static pressure important to the level.

The stronger flow up the right side of the mold is seen to raise the predicted surface pressure and corresponding level height near the narrow face. This height, or "standing wave", varies greatly between sides due to the initial biased flow condition. This might cause uneven consumption of the flux and change the lubrication and heat transfer conditions between the strand surfaces and mold walls. An oscillation of the surface pressure (and corresponding surface level profile) is predicted but the magnitude is quite small, as shown in Fig. 7. This small cyclic variation in the surface level appears to have a similar period to the oscillations in the lower recirculation zones.

Figure 3 illustrates the predicted melt turbulent kinetic energy (K). Maxima of K occur at each nozzle port, due to the strong shear layer around each incoming jet. Maxima also appear where the jets impinge at the narrow face walls. At these points, the local generation of turbulence is greater than the transport of turbulence from the vicinity. Figure 3 b)–f) shows a weak oscillation in the K fields, corresponding to the flow oscillations, but greatly diminished. This is also illustrated in Fig. 8. Using the correlation presented in the next section, this figure also predicts a maximum difference of 10 mm in the average height of surface level fluctuations. The variation in velocity and turbulence levels from left to right sides of the mold and with time together shows how slag entrainment and corresponding slab surface quality might vary from side to side.

The effect of the transient flow on melt heat transfer is stronger than on turbulence, as shown in Figs 4 and 9. The relatively higher temperature zone in the lower right vortex sheds and transports warmer liquid deeper into the lower strand, as it follows the flow, Fig. 4 c) and d). However, Fig. 9 shows that the magnitude of this effect is small. The initial temperature difference at the top surface due to biased flow is only about 1 and this is damped away quickly. This is because heat transfer is controlled more by turbulence than by time-averaged convection, especially in the slow lower region of the strand.

PREDICTION OF LEVEL FLUCTUATION BY STEADY STATE MODEL

Fluctuations of the top surface level are known to be very detrimental to steel quality. They may lead to entrainment of liquid mold flux [8], surface depressions and even cracks [11]. Ideally, level fluctuations could be modeled using a direct simulation method or a large eddy simulation method to solve for the instantaneous velocities while tracking the motion of the free surface. This is very difficult to achieve with current computer capacities, considering the other complex flow phenomena present in steel continuous casting processes. In this work, an easier method was sought.

A simple correlation is proposed between the time-averaged magnitude of the level fluctuations and the fluctuation energy predicted by the modified K–ε model for steady state flows. Random fluctuations in the turbulent motion of the swirling

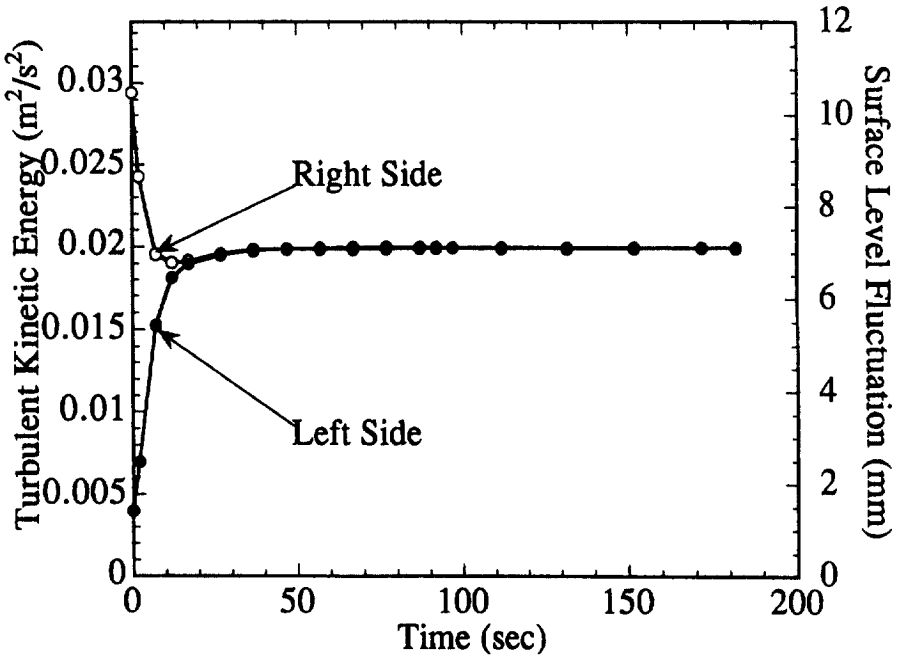

Fig. 8. Variation of predicted turbulent kinetic energy with time at the meniscus (shown with correlated surface level fluctuation).

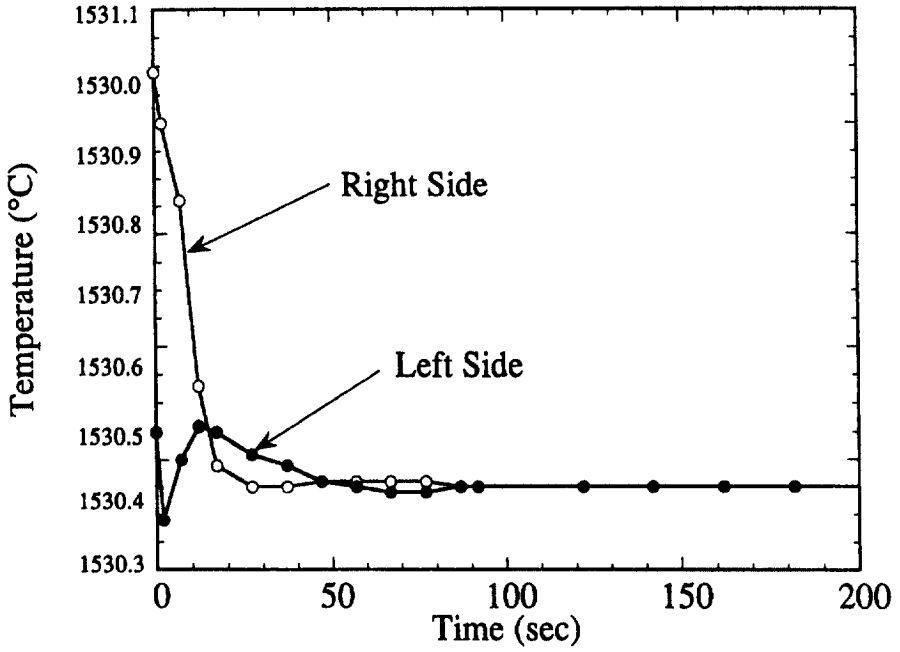

Fig. 9. Variation of melt temperature with time at the meniscus.

eddies is presumed to be responsible for level fluctuations. An ideal conversion from K to gravitational potential energy was assumed along the top surface. Equating these two energies yields:

$$\rho_l K = 0.5(\rho_l - \rho_f)gh \quad (1)$$

In this simple model, K represents the turbulent kinetic energy contained in the swirling eddies per unit mass of fluid and h is the distance from the peak to the trough of the average level fluctuation, h. To raise a volume of steel with density ρ_l above the interface as a level fluctuation, the gravitational potential energy must displace an equivalent volume of liquid flux, with density ρ_f. This gives rise to the $(\rho_l - \rho_f)$ term and g is acceleration due to gravity. The factor 0.5 takes into account that

Table 2. Simulation conditions for surface turbulence calculation by the modified K–ε model

Parameters	Values	
	Teshima [31] Case 1 (Base case)	Teshima [31] Case 2†
d_b, gas bubble size	3 mm	—
h_a, heat transfer coefficient at top surface	40 W/m^2 K	—
k_l, thermal conductivity	26 W/m K	—
K_0, turbulent kinetic energy at mold inlet	0.0666 m^2/s^2	0.137 m^2/s^2
SD, SEN submergence depth	0.180 m	—
W, mold width	0.9 m (35.4 in)	1.25 m (49.2 in)
N, mold thickness	0.203 m (8 in)	—
Q_g, inlet gas volume flow rate	1.69×10^{-4} m^3/s (8 SLM)	—
Sc_t, turbulent Schmidt Number	1	—
T_a, ambient temperture	27°C	—
T_0, pouring temperture	1550°C	—
v_c, casting speed	26.7 m/s (1.6 m/min)	34.5 m/s (2.1 m/min)
α_0, nominal angle of nozzle port	25°	—
ε_0, turbulence dissipation rate at mold inlet	0.512 m^2/s^3	2.57 m^2/s^3
μ_l, liquid steel laminar viscosity	0.0055 kg/ s m	—
ρ_l, liquid steel density	7020 kg/m^3	—
ρ_f, molten flux density	3000 kg/m^3	—
σ_{g0}, inlet volume fraction of gas bubbles	0.11	0.07

†Unlisted values are the same as Case 1.

the average interface position, H, is displaced to $H \pm h/2$ by the wave amplitude, which is only half of the total level fluctuation, h. For typical densities, (Table 2) this equation yields the correlation, $h \approx (0.356\ \text{s}^2/\text{m})\ K$.

Model validation

This simple model was first applied to predict level fluctuations under the conditions used by Teshima *et al.* in experiments at NKK Corporation, Japan [6]. The predicted results are compared with these experimental measurements in Figs 10 and 11. The simulation conditions are given in Table 2. The caster had two strands, casting at 1.6 m/min through a 0.9 m wide mold (Case 1) and at 2.1 m/min through a 1.25 m mold (Case 2). The same argon flow rate of 8 SLM (8 l/min at standard conditions of 1 atm pressure and 25°C) was used on both strands. The terms "south wide face" and "north wide face" in figs 10 and 11 indicate measurements near the two opposing wide face mold walls of each strand.

The predicted results show encouraging agreement with the measurements in Figs 10 and 11. This implies that the crude correlation between turbulent kinetic energy at the surface and level fluctuation may have some validity. It was expected that the dissipation process that converts turbulence into potential energy should be incomplete. After a level fluctuation has started, however, additional energy input is needed only to balance the loss of potential energy from the fluctuating wave due to damping dissipation. The agreement obtained using this simple model implies that these two dissipation rates are probably similar.

Both predictions and measurements show that the combined effects of casting speed and mold width change the nature of the level fluctuations. The maximum level fluctuation is located near the mold center for Case 1 (the base case with a narrow mold and low casting speed). It moves to near the narrow face wall for Case 2 (a wide mold at a higher casting speed). This effect is due to the increased importance of the argon directing flow towards the surface when the steel flow rate is lower, as discussed in further detail below.

There are obvious discrepancies between the predictions and the experiments. Firstly, the model consistently predicts stranger level fluctuation at the wide face centerline than near the wide face walls, while the opposite tendency was measured in the experiments. This is expected because the effect of mold oscillation, which was ignored in the mold, should be strongest near the mold walls. Secondly, the model underpredicts the measured level fluctuations near the narrow face for Case 1 and overpredicts them near the SEN for Case 2. It should be pointed out that the viscous molten flux layer strongly affects the flow along the top surface, which has been neglected in the present model. The molten flux reduces surface velocities of the steel by about 75% [40]. Its effect on kinetic energy is expected to be much less, but is likely one of the reasons for the discrepancy between the predictions and measurements. Nevertheless, the favorable comparison with results from this unrefined model are encouraging.

Having somewhat validated the model, it is next applied to explore the effect of casting conditions, including argon gas injection rate, submergence depth of the submerged entry nozzle (SEN), and casting speed.

Parametric study

The rate of argon gas injection significantly affects the surface turbulence and level fluctuation. This is shown in Fig. 12. Increased argon fraction generally increases both surface turbulence and level fluctuations. Argon also changes the steel flow pattern, however, which changes where the maximum steel velocities impinge upon the surface. This, in turn, alters the distribution of turbulence and level fluctuation across the mold width. Adding 11% argon with the steel entering the mold raises the surface turbulence and level fluctuations near the mold

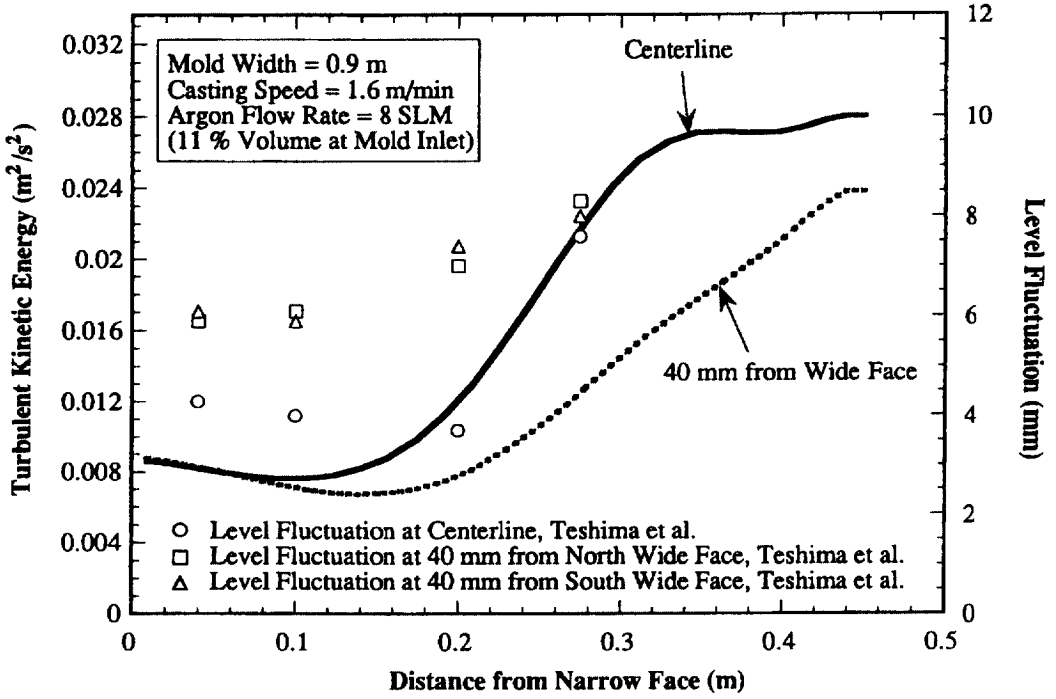

Fig. 10. Comparison of predicted turbulent kinetic energy and measured surface level fluctuation (Case 1 in Table 2).

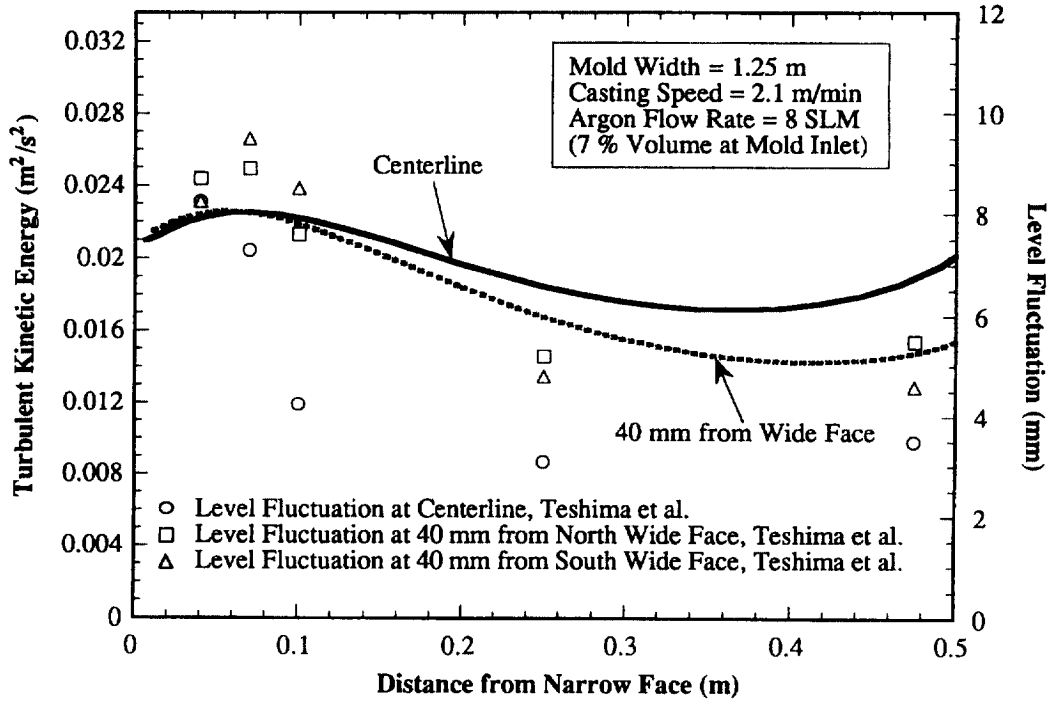

Fig. 11. Comparison of predicted turbulent kinetic energy and measured surface level fluctuation (Case 2 in Table 2).

center by almost four times. When no argon is injected (the two thinner curves in Fig. 12), level fluctuations are strongest near the wall. This is because the steel jet impinges first upon the narrow face, before being directed upward and impacting the top surface near the narrow face.

These results explain the differences observed between Cases 1 and 2 in Figs 10 and 11. Increasing mold width and casting speed increases both the speed and flow rate of the molten steel. For the same argon flow rate, the higher steel flow rate lowers the fraction of argon entering the mold from 11% for Case 1

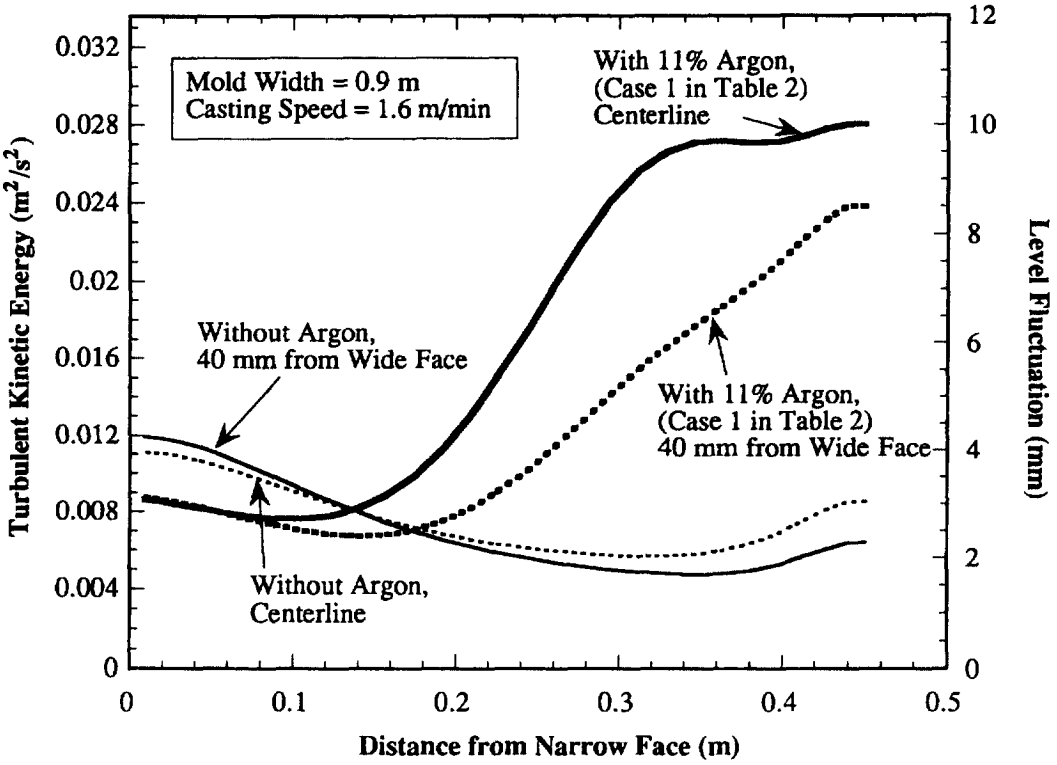

Fig. 12. Effect of argon on predicted turbulent kinetic energy and correlated surface level fluctuation.

to 7% for Case 2. When combined with the further penetration of the higher speed jet across the mold width, this changes the flow pattern. Instead of rising to the free surface and moving towards the narrow face, the high-speed, low-argon jet first impacts the narrow face wall below the surface. The jet rises up the narrow face to flow back across the top surface towards the SEN, with corresponding changes in the surface level and level fluctuation maxima. Other conditions being equal, this finding suggests that varying argon injection rate directly with steel flow rate should tend to make flow in the mold more uniform.

The submergence depth (SD) of the SEN has an important effect on surface turbulence, as shown in Fig. 13. Deeper submergence generally decreases surface turbulence, which matches findings in practice. Specifically, level fluctuations are predicted to decrease by a factor of two when submergence is lowered from 100 to 180 mm. Further deepening the SD to 260 mm has less effect, however. This is because lowering the SEN below a critical level changes the flow pattern to make the jet first impinge upon the narrow face. Further decreases in depth are not particularly effective at lowering the velocity of the high speed jet which flows up the narrow face wall and recirculates back across towards the SEN. This critical depth varies with operating conditions.

Increasing casting speed tends to increase level fluctuations, assuming other conditions and the flow pattern remain constant. This is because the velocity of the steel moving across the interface was found to increase proportionally with casting speed, which produces an increase in both turbulent kinetic energy levels and gradients. Specifically, increasing speed from 1.0 to 1.6 m/min increased maximum surface velocity from 0.04 to 0.09 m/s which increased K from 0.008 to 0.020 m^2/s^2 and increased h from 3 to 7 mm. This prediction qualitatively matches the well-known experience in practice. This is one of the important problems that limits higher casting speed.

CONCLUSIONS

(1) A 3D, 2-phase, turbulent finite difference model has been developed to simulate transient flow behavior in steel continuous casting processes, including the important effects of argon gas bubbles. It has been applied to simulate the transition from steady biased flow to steady symmetrical flow.

(2) The results illustrate shedding of the large lower vortex. A corresponding low-frequency oscillation of the flow and thermal pattern was predicted by the model, although these were quickly damped. The magnitude of the turbulent kinetic energy and temperature distributions in the liquid were least affected by this oscillation in the lower zone. No drastic sloshing was predicted even though the tangential velocities were free to change. The transition from uneven to even flow takes about 90 s.

(3) Turbulent kinetic energy predicted by the modified, steady-state K–ε model can be easily transformed to predict surface level fluctuations, which roughly agree with measurements [6].

(4) Typical argon injection rates not only greatly raise the surface turbulence intensity, but also alter the turbulence distribution. The combined effect of mold width and casting

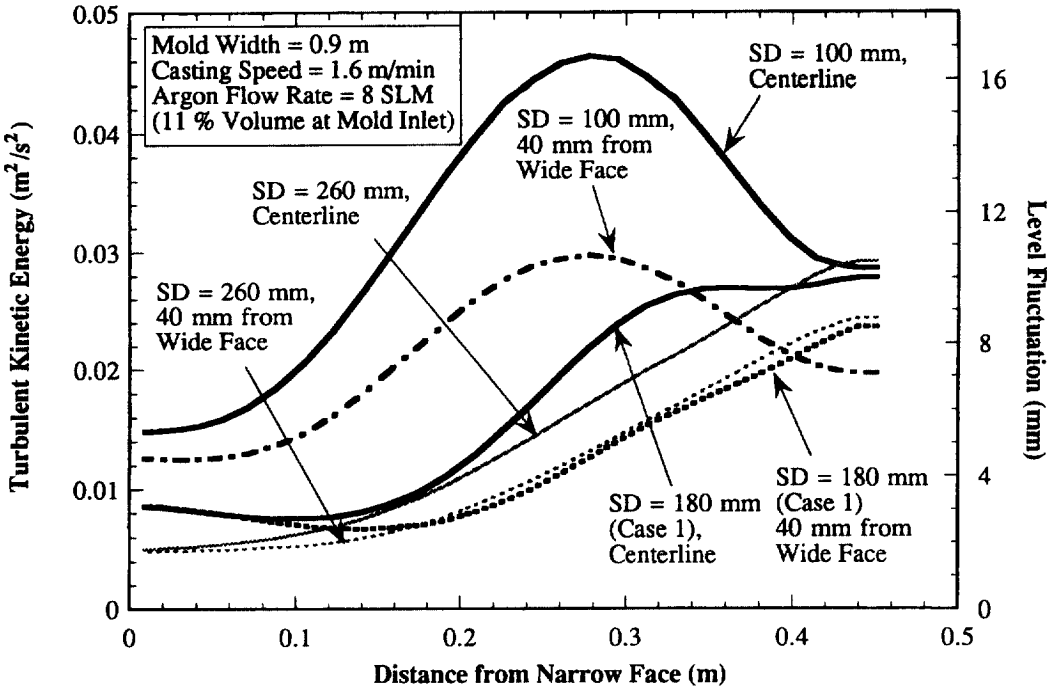

Fig. 13. Effect of submergence depth on predicted turbulent kinetic energy and correlated surface level fluctuation.

speed on measured surface level behavior can be explained by including the change in flow rate on the argon fraction.

(5) The effect of casting conditions on surface level fluctuations can be predicted. Surface turbulence and level fluctuations are decreased by increasing nozzle submergence depth or decreasing casting speed.

APPENDIX I

Model equation details

Conservation equations for mass continuity, momentum, energy transport, and a modified two-equation K–ε turbulence model, were solved for the molten steel–bubble mixture parameters. The first three equations are based on standard volume averaging [24, 25] and Reynolds time averaging techniques [26, 27] and are given in Cartesian tensor form as:

$$\frac{\partial}{\partial x_j}(\rho v_j) = 0 \tag{1}$$

$$\frac{\partial}{\partial t}(\rho v_i) + \frac{\partial}{\partial x_j}(\rho v_j v_i) = -\frac{\partial p}{\partial x_i} + \frac{\partial}{\partial x_j}\left[\mu_{\text{eff}}\left(\frac{\partial v_i}{\partial x_j} + \frac{\partial v_j}{\partial x_i}\right)\right] + \rho g_i \tag{2}$$

$$\frac{\partial}{\partial t}(\rho C_p T) + \frac{\partial}{\partial x_j}(\rho v_j C_p T) = \frac{\partial}{\partial x_j}\left(k_{\text{eff}}\frac{\partial T}{\partial x_j}\right) \tag{3}$$

where ρ, v_i (or v_j), T, C_p are, respectively, the density, velocity component, temperature and specific heat of the mixture, defined as:

$$\rho \equiv (1-\sigma_g)\rho_l + \sigma_g \rho_g \tag{4}$$

$$\rho v_i \equiv (1-\sigma_g)\rho_l v_{li} + \sigma_g \rho_g v_{gi} \tag{5}$$

$$T \equiv (1-\sigma_g)T_l + \sigma_g T_g \tag{6}$$

$$\rho C_p \equiv (1-\sigma_g)\rho_l C_{pl} + \sigma_g \rho_g C_{pg} \tag{7}$$

Inserting typical gas ($_g$) and liquid ($_l$) properties into these definitions reveals that the velocity components, temperature, and heat content of the liquid phase are virtually the same as that of the mixture, which greatly simplifies the model. The apparent density change of the mixture due to the bubbles was ignored in this simplified two-phase model, which is reasonable when the bubble volume fraction, σ_g, is less than 5%.

The transport coefficients, the effective kinetic viscosity μ_{eff} and effective thermal conductivity k_{eff}, each include two components:

$$\mu_{\text{eff}} = \mu_0 + \mu_t \tag{8}$$

$$k_{\text{eff}} = k_0 + \frac{C_p \mu_t}{Pr_t} \tag{9}$$

The turbulent Prandtl number, Pr_t, is set to the standard value of 0.9. Arithmetic averaging is used to calculate the molecular components of viscosity μ_0 and thermal conductivity k_0:

$$\mu_0 \equiv (1-\sigma_g)\mu_{0l} + \sigma_g \mu_{0g} \tag{10}$$

$$k_{\text{eff}} \equiv (1-\sigma_g)k_{0l} + \sigma_g k_{0g} \tag{11}$$

Extra source terms were introduced into the standard K–ε turbulence equations to account for the enhanced mixture turbulence caused by the bubbles, based on the model of Malin and Spalding [28] for mixing of cold and hot gases:

$$\frac{\partial}{\partial t}(\rho K) + \frac{\partial}{\partial x_j}(\rho v_j K) = \frac{\partial}{\partial x_j}\left(\frac{\mu_t}{\sigma_K}\frac{\partial K}{\partial x_j}\right)$$

$$+\rho G_K-\rho\varepsilon+C_{K1}\sigma_g(1-\sigma_g)G_K+C_{K2}C_f\sigma_g\rho_l K \quad (12)$$

$$\frac{\partial}{\partial t}(\rho\varepsilon)+\frac{\partial}{\partial x_j}(\rho v_j\varepsilon)=\frac{\partial}{\partial x_j}\left(\frac{\mu_t}{\sigma_\varepsilon}\frac{\partial\varepsilon}{\partial x_j}\right)+C_1\frac{\varepsilon}{K}\rho G_K-C_2\frac{\varepsilon}{K}\rho\varepsilon$$

$$+C_{\varepsilon l}\sigma_g(1-\sigma_g)\frac{\varepsilon}{K}\rho G_K+C_{\varepsilon 2}+C_{\varepsilon 2}C_f\sigma_g\rho_l\varepsilon \quad (13)$$

$$G_K=\frac{\mu_t}{\rho}\frac{\partial v_j}{\partial x_i}\left(\frac{\partial v_i}{\partial x_j}+\frac{\partial v_j}{\partial x_i}\right) \quad (14)$$

The turbulent viscosity μ_t is defined in the standard way:

$$\mu_t=c_{\mu\rho}\rho\frac{K^2}{\varepsilon} \quad (15)$$

The standard constants in this modified K–ε model are:

$$C_1=1.44,\quad C_2=1.92,\quad C_\mu=0.09,\quad \sigma_K=1.0,\quad \sigma_\varepsilon=1.3 \quad (16)$$

The four extra empirical constants needed in this modified K–ε model were taken from Sheng and Irons [31], who reported a better match with experiments in bubbly molten metal flows by increasing the original constants [28] to the following values:

$$C_{K1}=4.0,\quad C_{K2}=0.6,\quad C_{\varepsilon 1}=6.0,\quad C_{\varepsilon 2}=0.75 \quad (17)$$

C_f is a friction factor, defined from the bubble diameter, d_b, and the vertical component of the bubble terminal velocity, v_{gtz}:

$$C_f=\frac{3}{4d_b}C_D v_{gtz} \quad (18)$$

The bubble drag coefficient, C_D, is found from Stoke's law, modified for bubbly flow using the following empirical function of Reynolds number:

$$C_D=\frac{24}{Re}(1+0.15Re^{0.687})(1-\sigma_g)^{-1.7},\quad Re\leqslant 1000 \quad (19)$$

$$C_D=0.44,\quad Re>1000 \quad (20)$$

and

$$Re=\frac{d_b\rho_l v_{gtz}}{\mu_{0l}} \quad (21)$$

The bubble terminal velocity, v_{gtz} was defined by an empirical relation from Soo and Szekely [24, 41] which was based on a compilation of experimental measurements from different researchers for bubble sizes up to 10 mm:

$$v_{gtz}=\exp(a_0)\exp(a_1\ln d_g)\exp[a_2(\ln d_g)^2]$$

$$a_0=-8.373,\quad a_1=-2.6306,\quad a_2=-0.2500 \quad (22)$$

Bubble dispersion due to turbulent transport in the mixture is calculated by solving a continuum transport equation of σ_g [21]:

$$\frac{\partial}{\partial t}-(\sigma_g)+\frac{\partial}{\partial x_j}(\sigma_g(v_j+V_{gtj}))=\frac{\partial}{x_j}\left(D_g\frac{\partial\sigma_g}{\partial x_j}\right) \quad (23)$$

where the "diffusivity" of the bubbles in the mixture, D_g, is assumed to be equal to the turbulent diffusivity of a solute element and the turbulent Schmidt Number, Sc_t, is set to 1:

$$D_g=\frac{\mu_t}{\rho Sc_t}=\frac{\mu_t}{\rho} \quad (24)$$

Acknowledgements—The authors wish to thank AK Steel, Allegheny Ludlum, Armco Inc., LTV Steel, Inland Steel Co., BHP, Stollberg and the National Science Foundation, (DMI-9800274) for funding and NCSA for supercomputing time.

REFERENCES

1. Huang, X. and Thomas, B. G., Modeling of steel grade transition in continuous slab casting processes. *Metallurgical Transactions*, 1993, **24B**, 379–393.
2. Lawson, G. D., Sander, S. C., Emling, W. H., Moitra, A. and Thomas, B.G, Prevention of shell thinning breakouts associated with widening width changes. *Steelmaking Conference Proceedings*, 77, Iron and Steel Society, Warrendale, PA, 1994, pp. 329–336.
3. Moitra, A., Thermo-mechanical model of steel shell behavior in continuous casting. Ph.D. thesis, University of Illinois at Urbana-Champaign, 1993.
4. Brimacombe, J. K., Empowerment with knowledge—toward the intelligent mold for the continuous casting of steel billets. *Metallurgical Transactions B*, 1993, **24B**, 917–935.
5. Perkins, A., Brooks, M. G. and Haleem, R. S., Roll performance in continuous slab casting machines. *Ironmaking and Steelmaking*, 1985, **12**(6), 276–283.
6. Teshima, T., Osame, K., Okimoto, K. and Nimura, Y., Improvements of surface property of steel at high casting speed. *Steelmaking Conference Proceedings*, 71, Iron and Steel Society, Warrendale, PA, 1988, pp. 111–118.
7. Honeyands, T. and Herbertson, J., Flow dynamics in thin slab caster moulds. *Steel Research*, 1995, **66**(7), 287–293.
8. Emling, W. H., Waugaman, T. A., Feldbauer, S. L. and Cramb, A. W., Subsurface mold slag entrainment in ultra-low carbon steels *Steelmaking Conference Proceedings*, 77, Chicago, IL, Iron and Steel Society, Warrendale, PA, 1994, pp. 371–379.
9. Kumar, S., Walker, B. N., Samarasekera, I. V. and Brimacombe, J. K., Chaos at the meniscus–the genesis of defects in continuously cast steel billets. *PTD Conference Proceedings*, 13, Iron and Steel Society, Warrendale, PA, 1995, pp. 119–141.
10. Jenkins, M. S., Thomas, B. G., Chen, W. C. and Mahapatra, R. B., Investigation of strand surface defects using mold instrumentation and modeling. *Steelmaking Conference Proceedings*, 77, Iron and Steel Society, Warrendale, PA, 1994, pp. 337–345.
11. Thomas, B. G. and Zhu, H., Thermal distortion of solidifying shell in continuous casting of steel. In *Proceedings of International symposia on Advanced Materials and Technology for the 21st Century*, eds. I. Ohnaka and D. Stefanescu. TMS, Warrendale, PA, Honolulu, HI; 1996, pp. 197–208.
12. Yasunaka, H., Taniguchi, K., Kokita, M. and Inoue, T., Surface quality of stainless steel type 304 cast by twin-roll type strip caster. *Iron and Steel Institute of Japan*, 1995, **35**(6), 784–789.
13. Kubota, J., Okimoto, K., Shirayama, A. and Murakami, H., Meniscus flow control in the mold by travelling magnetic field for high speed slab caster. In *Mold Operation for Quality and Productivity*, eds. A. W. Cramb and E. Szekeres. Iron and Steel Society, Warrendale, PA, 1991.
14. Huang, X. and Thomas, B. G., Intermixing model of continuous casting during a grade transition. *Metallurgical Transactions B*, 1996, **27B**(4), 617–632.
15. Thomas, B. G., Modeling study of intermixing in tundish and strand during a continuous-casting grade transition. *ISS Transactions*, 1996, **24**(12), 83–96.
16. Damle, C. and Sahai, Y., Modeling of grade change operations during continuous casting of steel—mixing in the tundish. *Iron and Steelmaker (ISS Transactions)*, 1995, **22**(6), 49–59.
17. Chen, H. and Pehlke, R. D., Minimization of transition slabs based on tundish flow control. *Steelmaking Conference Proceedings*, 77, Iron and Steel Society, Warendale, PA, 1994, 695–702.
18. Austin, P. R., Camplin, J. M., Herbertson, J. and Taggart, I. J.,

Mathematical modeling of thermal stratification and drainage of steel ladles. *Iron and Steel Institute of Japan International*, 1992, **32**(2), 196–202.
19. Chakroborty, S. and Sahai, Y., Mathematical modeling of transport phenomena in continuous casting tundishes part 1. Transient effects during ladle transfer operations. 1992, **19**(6), 479–487.
20. Huang, X., In *Mathematical Models of Continuous Casting of Steel Slabs, Annual Report to Continuous Casting Consortium*, ed. B. G. Thomas. University of Illinois, Urbana, IL; 1993.
21. Thomas, B. G., Huang, X. and Sussman, R. C., Simulation of argon gas flow effects in a continuous slab caster. *Metall. Trans. B.*, 1994, **25B**(4), 527–547.
22. Patankar, S. V., *Numerical Heat Transfer and Fluid Flow*, McGraw–Hill, New York, 1980.
23. Huang, X., Studies on turbulent gas-particle jets and 3D turbulent recirculating gas-particle flows. Ph.D. thesis, Tsinghua University, Beijing, P.R. China, 1988.
24. Soo, S. L., *Fluid Dynamics of Multiphase System, Chapter* 3: *Transport Processes of a Deformable Particle*, Blaisdell Publishing Co., Waltham, MA, 1967.
25. Ishii, M., *Thermo-Fluid Dynamic Theory of Two-Phase Flow*, Eyrolls, Paris, 1975.
26. Hinze, J. O., *Turbulence*, McGraw–Hill, New York, 1975.
27. Schlichting, H., *Boundary-Layer Theory*, McGraw–Hill, New York, 1979.
28. Malin, M. R. and Spalding, D. B., A two-fluid model of the turbulence and its application to heated plane jet and wakes. *Physico Chemical Hydrodynamics*, 1984, **5**(5-6), 339–362.
29. Burty, M., Fautrelle, Y. and Huin, D., A computational model for the prediction of turbulent recirculating two-phase flows in a gas-stirred steel ladle. In *Proceedings of the 6th International Iron and Steel Congress*. 1, ed. Y. Yagi, ISIJ, Tokyo, Nagoya, Japan, 1990, pp. 444–465.
30. Ilegbusi, O. J. and Szekely, J., The modeling of gas-bubble driven circulation systems. *Iron and Steel Institute of Japan International*. 1990, **30**(9), 731–739.
31. Sheng, Y. Y. and Irons, G. A., Turbulence modeling of plume flows in a gas stirred ladle. *Process Technology Conference* (*75th Steelmaking Conference*), 1992. Toronto, Ontario, Canada, The Iron and Steel Society, Warrendale, PA.
32. Huang, X., Thomas, B. G. and Najjar, F. M., Modeling superheat removal during continuous casting of steel slabs. *Metallurgical Transactions B*, 1992, **23B**(6), 339–356.
33. Hershey, D. E., Thomas, B. G. and Najjar, F. M., Turbulent flow through bifurcated nozzles. *International Journal for Numerical Methods in Fluids*, 1993, **17**, 23–47.
34. Launder, B. E. and Spalding, D. B., Numerical computation of turbulent flows. *Computer Methods in Applied Mechanics and Engineering*, 1974, **13**, 269–289.
35. Thomas, B. G. and Najjar, F. M., Finite-element modeling of turbulent fluid flow and heat transfer in continuous casting. *Applied Mathematical Modeling*, 1991, **15**, 226–243.
36. Birat, J. P., Etude experimentale des jrs confines dans le cas de l'introduction d'acier liquide en lingotiere de coulee continue de brames. Presented at *3rd Congres de Mecanique Francais*, Grenoble, 6–9 September 1977.
37. Gupta, D. and Lahiri, A. K., A water model study of the flow asymmetry inside a continuous slab casting mold, *Metallurgical and Materials Transactions*, 1996, **27B**(5), 757–764.
38. Ho, B., Characterization of interfacial heat transfer in the continuous slab casting process. Masters thesis, University of Illinois at Urbana-Champaign, 1992.
39. McDavid, R., Fluid flow and heat transfer behavior of top-surface flux layers in steel continuous casting. Masters thesis, University of Illinois at Urbana-Champaign, 1994.
40. McDavid, R. and Thomas, B. G., Flow and thermal behavior of top-surface flux/powder layers in continuous casting molds. *Metallurgical Transactions B*, 1996, **27B**(4), 672–685.
41. Szekely, J., *Fluid Flow Phenomena in Metals Processing*, Academic Press, Inc., New York, 1979.